Regular Article

PHYSICAL CHEMISTRY RESEARCH
Published by the
Iranian Chemical Society
www.physchemres.org
info@physchemres.org

Phys. Chem. Res., Vol. 10, No. 3, 301-313, September 2022
DOI: 10.22036/PCR.2021.303554.1968

Adsorption of the Methylene Blue Dye in Environmental Water Samples by Biochar Obtained from the Valorization of Argan Shells

A. Ouedrhiri*, Y. Lghazi, J. Bahar, M. Ait Himi, C. El Haimer, B. Youbi, M. Khoukhi and I. Bimaghra

Bio-Geosciences and Materials Engineering Laboratory, Ecole Normale Superieure, Hassan II University of Casablanca, Morocco, 50069

(Received 18 September 2021, Accepted 21 November 2021)

Biochar is an adsorbent material widely used to remove pollutants from industrial discharges. This research focuses on the adsorption capacity of Biochar, obtained by thermal decomposition of Argan shells, to remove methylene blue from aqueous solutions. The influence of some parameters such as carbonization time and temperature on the burn-off and adsorption capacities of this material was studied. A temperature of carbonization of 900 °C and a carbonization time of 2 h is considered as the optimum conditions for the preparation of this adsorbent. The burn-off, methylene blue adsorption amount, and iodine number of the prepared activated carbon under the optimal conditions were 84.6 %, 19.9 mg g^{-1}, and 431.8 mg g^{-1}, respectively. The powder obtained was characterized by performing the following analyses: pH_{pzc}, SEM, FT-IR, DRX, and TGA-DTG. It was then tested for its ability to remediate methylene blue in water by varying the carbon dosage, contact time, initial concentration, and pH. The adsorption kinetics was consistent with the pseudo-second-order model. To analyze the experimental data, Langmuir, Freundlich, and Temkin models were studied. The equilibrium data are in agreement with the Langmuir model with a monolayer maximum adsorption capacity of 31 mg g^{-1}.

Keywords: Adsorption, Biochar, Argan shells, Kinetics, Isotherms

INTRODUCTION

For a long time, most industrial companies use different types of dyes in the production process, but the rest (residual or unused) is released into nature like any other pollutant [1]. Among the most used dyes in the industry is methylene blue (MB), a cationic dye generally found in the chemical or biological fields: pharmaceutical, food, plastics, and dyeing [2], but it can cause adverse effects on aquatic life and human health [3]. Because of its special structure, MB is highly soluble in aqueous solutions and almost non-biodegradable, it lasts for a long time in the environment [4]. Long-term exposure to this substance can cause several health problems such as tachycardia, vomit, cyanosis, gangrene, hypertension, jaundice, quadriplegia, and anemia [5]. For this cause, it is important to eliminate this type of pollutant from industrial discharges before they are evacuated into water streams.

Lately, different techniques are applied to the treatment of industrial waste containing dyes, including biological treatment, coagulation, flocculation, photocatalytic degradation, filtration, and adsorption [6].

Adsorption is very effective in terms of ease of implementation and design cost for the treatment of wastewater, containing dyes, with an adsorbent material. Because of the high cost and complicated preparation and regeneration procedures of these types of materials such as activated carbon (AC), the search for cheap and high-quality adsorbents continues. Naturel wastes have emerged as a better choice for developing AC. Currently, biochar (BC) is considered the most promising, efficient and used adsorbent for a wide range of pollutants, with high adsorption capacity

*Corresponding author. E-mail: ad.oudrhiri@gmail.com

[7,8].

Commercial AC has a high cost, this may be due to the method of production and the type of raw material, hence the interest to study the possibility of using less expensive raw materials with simple preparation means. Moreover, several natural residues such as coconut coir pith [9], apple peels [10], Avocado seed [11], peanut shells [12], olive solid waste [13], and sugarcane waste [14] have been investigated as BC precursors and have received special attention. In addition, the conversion of agricultural wastes into value-added AC offers a new route for its valorization.

Among the natural residues, we also find the Argan shells (AS) of the Argania Spinosa tree, which are recovered after the production of Argan oil. Argania Spinosa covers 70% of the surface of the southwest region of Morocco and the amount of AS waste generated annually is 2700 tons [15]. Hence the interest in the preparation of the activated carbon from Argan shells.

The preparation of AC is done either by physical activation, which requires the carbonization of the raw material followed by activation of the resulting carbon with carbon dioxide or steam. Or by chemical activation using activating agents (salts, acids, or bases), for example, $ZnCl_2$, H_3PO_4, and NaOH. In the chemical process, the yield of carbonization is higher and the temperature used is lower than in the physical process [16].

This work treats the preparation of an adsorbent from AS and the extensive characterization studies to evaluate its performance. The adsorptive property of this material was tested by the adsorption of MB from an aqueous solution. The influence of several operational parameters such as contact time, adsorbent dosage, initial concentration, and pH was studied. Kinetics studies and adsorption isotherm models were also investigated.

MATERIALS AND METHODS

Materials

The AS collected in southern Morocco were sorted and washed with distilled water several times to obtain a raw material without impurities. Then, passed to the oven at 100 °C until complete drying. The well-dried shells were crushed and sieved to retain the 500 µm fraction, which was then introduced into the furnace without any chemical activation.

Carbonization of Argan Shells

To prepare the biochar, a mass of 60 g of clean and dry AS introduced in a well-closed crucible, positioned in the furnace, was carbonized at a rate of 10 °C min^{-1} at various temperatures ranging from 500-900 °C and for different times 1 h, 2 h, and 3 h. At the end of this step, the crucible is allowed to cool to room temperature before recovering the carbonized sample.

The burn-off is calculated using the following equation:

$$Burn\ off\ (\%) = \frac{M_0 - M}{M_0} \times 100 \quad (1)$$

Where M_0 is the weight of the dried raw material and M is the weight of the Biochar.

Characterization of the Biochar

The iodine adsorption was performed using the sodium thiosulphate volumetric method, according to the procedure defined by ASTM D4607- 94(2006) [17].

The crystal structure of the BC was determined using a BRUKER D8 ADVANCE diffractometer with radiation K_α (λ = 0.154 nm) equipped with a curved position-sensitive detection. The surface functionalities were investigated with Fourier Transform InfraRed (FTIR) spectroscopy (IRAffinity-1S). Thermo-Gravimetric analysis (TGA) and Derivative Thermo-Gravimetric (DTG) were performed by using a derivatograph (DTG-60H SHIMADZU). 7.685 mg of crushed AS was heated up to 1000 °C at a heating rate of 10 °C min^{-1}. The surface morphology of AC was characterized by using the Scanning Electron Microscopy (SEM) under SH-(4000M HIROX) microscope with a 5 Kv accelerating voltage.

The point of neutral electric charge of the adsorbent surface was obtained by the solid addition method [18,19]. The manipulation was carried out in beakers of 50 ml. Volumes of 20 ml of 0.1 M KNO_3 solutions of different initial pH were transferred to the beakers containing 0.20 g of AC. The initial pH values of the KNO_3 solutions were adjusted between 2 and 12 by adding 0.1 M NaOH or 0.1 M HCl. The final mixture is agitated under a stirring speed of 140 rpm for one day.

Adsorption of Methylene Blue

Methylene blue (CI 52015), the adsorbate used in all experiments, whose chemical formula $C_{16}H_{18}ClN_3S$ and MW = 319.85 g mol^{-1} [20] was prepared by distilled water. The maximum absorbance (λ_{max}) of MB determined using a UV-Vis spectrophotometer (UV-1800, Bejing Rayleigh Co., Ltd.) and chemical structure, are shown in Fig. 1.

The adsorption study was performed at 25 °C by mixing different masses of BC with 100 ml of the MB solution with a concentration range of 20-100 mg l^{-1} under a stirring speed of 400 rpm.

The adsorption percentage R (%) of MB was calculated using the following expression:

$$R\,(\%) = \frac{C_0 - C_e}{C_0} \times 100 \qquad (2)$$

The amount of MB adsorbed at equilibrium q_e (mg g^{-1}) was calculated by the following equation:

$$q_e = \frac{V(C_0 - C_e)}{W} \qquad (3)$$

Where C_0 is the initial concentration (mg l^{-1}), C_e is the equilibrium concentration of MB (mg l^{-1}), V is the volume of the solution (l), and W is the weight of the adsorbent (g).

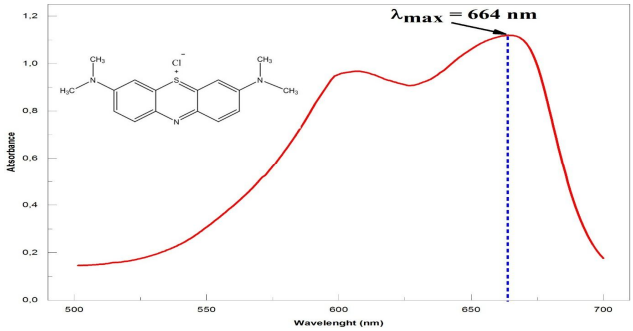

Fig. 1. The chemical structure and UV-Vis spectrum of MB solution (100 mg l^{-1}).

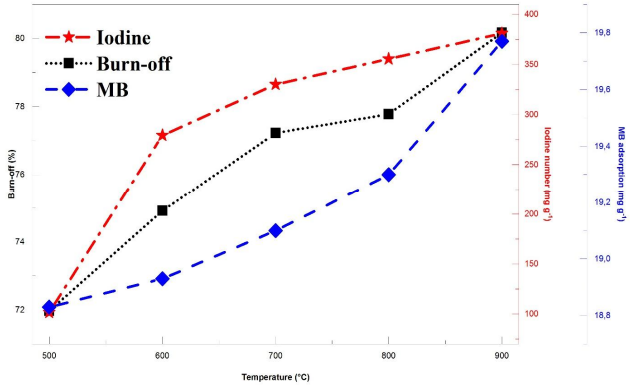

Fig. 2. The effect of carbonization temperature on the Burn-off and adsorption capacities of Biochar (t_c = 1 h).

RESULTS AND DISCUSSION

Preparation of Biochar from AS

Effect of carbonization temperature. The influence of the carbonization conditions plays a most important role on the activated carbon characteristics and allows to determine the optimal preparation conditions. The Effect of carbonization temperature (T_c) on the adsorption efficiency and the Burn-off was studied with a carbonization time (t_c) of 1 h (Fig. 2). As can be seen, the thermal activation degree of BC increased from 72 to 80.2% with the increase of carbonization temperature from 500 °C to 900 °C.

A similar observation of the amount of MB and iodine number increasing from 18.83 to 19.77 mg g^{-1} and 101 to 381 mg g^{-1}, respectively. The iodine molecule informs that the surface of the material contains pores with a diameter greater than 1 nm [21]. In contrast, pores with a diameter greater than 1.5 nm adsorb MB molecules [22]. The T_c = 900 °C was chosen to prepare the Biochar from the Argan shells.

Effect of carbonization time. The effect of carbonization time on the adsorption efficiency and the Burn-off of activated carbon was studied with the 900 °C temperature (Fig. 3). It was observed that the burn-off of material increased from 80.17 to 86.4% when the carbonization time was extended from 1 to 3 h. The same is observed for the amount adsorption of MB and the iodine number. It seems that the variation of these quantities depends on the thermal activation time. However, prolonging the activation time would promote the formation of many more active sites and pores on the surface of the substrate. The t_c considered is 2 h and the AS sample

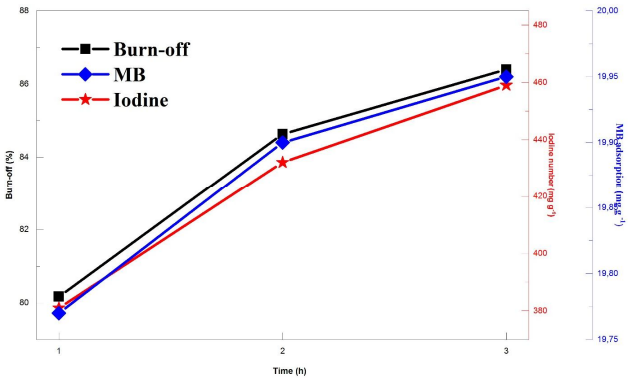

Fig. 3. The effect of carbonization time on burn-off and adsorption capacities of Biochar (T_c = 900 °C).

carbonized under the optimal conditions of temperature and time is designated AS-C92.

Characterization of Biochar

SEM analysis of microstructure. The SEM was employed to analyze the surface morphology of the Argan shells before and after thermal activation at T_c = 900 °C for 2h. The obtained images are shown in Fig. 4. As can be seen, the AS (Fig. 4a) presents a homogeneous, uniform, and smooth surface. In contrast, the AS-C92 (Fig. 4b) has a rough surface with much larger and irregularly sized cavities. These results show that the activation at the optimum operating condition resulted in visible changes in the pore structure of AS-C92. Similar changes have been observed preparing in Biochars from date seeds [23] and date stones [24]. The pore structure provides more adsorption sites for the dye which facilitates the penetration of the solution inside the adsorbent.

Functional Groups of AS-C92

In order to know the surface functional groups on the prepared materials, FTIR transmission spectra were studied (Fig. 5). The FTIR spectrum of Argan shells shows that there is an IR band at about 3312 cm^{-1}, which corresponds to the vibrations (O-H) of hydroxyl groups [25]. The bands at about 2926 and 2853 cm^{-1} are related to the vibrations (C-H) of methylene and methyl groups [26,27]. The peak at 2359 cm^{-1} corresponds to the (C≡C) vibrations of alkyne groups [28]. Another band that appears at 1740 cm^{-1} could

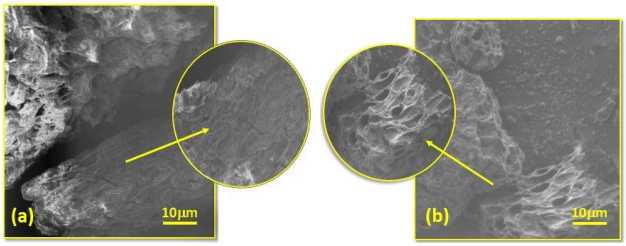

Fig. 4. SEM micrographs of the raw material (a) and the AS-C92 (b).

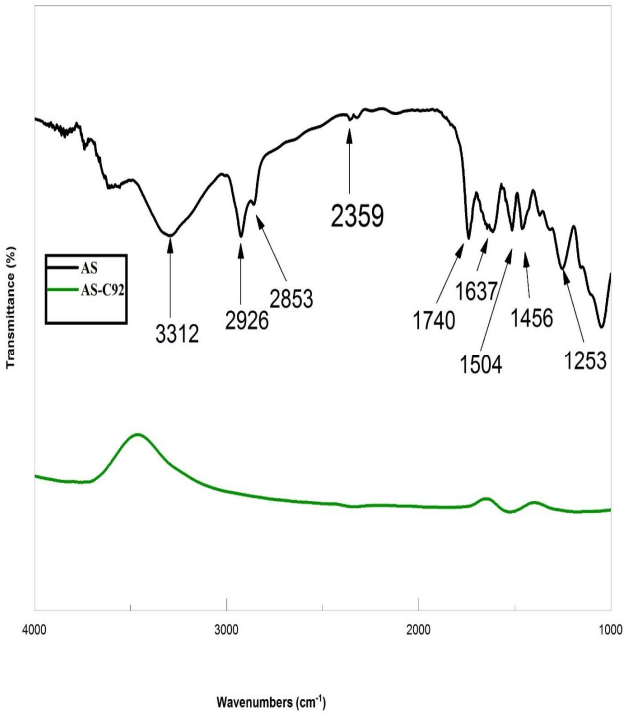

Fig. 5. FT-IR spectra of AS and AS-C92.

be related to the stretching vibrations (C=O) of carbonyl groups or ketones and the peak located at 1637 cm^{-1} corresponds to the aromatic bonds (C=C). On the other hand, the C=C stretching of aromatic cycle is relative to the peak located at 1504 cm^{-1} [29]. This observation is confirmed by the presence of the band at 1456 cm^{-1} of the C=C double bond of aromatic cycles [30]. Then, the bands between 1300 and 1000 cm^{-1} could be attributed to vibrations of the carbon-oxygen (C-O) single bond [31]. The band at 1504 cm^{-1} in the Biochar spectrum appears similar to that of the precursor. However, some of the peaks

after carbonization have disappeared. This could suppose that the majority of the functional groups were removed by the thermal activation.

TGA-DTG Analysis

To better understand the decomposition behavior during the carbonization stage, a thermal analysis was studied. The TGA and DTG curves are presented in Fig. 6 for dried Argan shells. The loss of mass is obtained in the temperature range of 36-1000 °C, which can be separated into four stages. At temperatures below 100 °C, we observe a first mass loss (11.39% by weight) corresponding to an endothermic loss and could be attributed to the vaporization of the water contained in the sample. Between 100 and 150 °C, a second mass loss (51.26% by weight) is observed which can be explained by the decay of organic matter. Above 150 °C, we observe the beginning of the thermal decomposition of the main elements of AS: from 150 to 360 °C, there is the degradation of the hemicellulose part, then between 360 and 460 °C that of the cellulose and beyond 460 °C that of the lignin (73.09% by weight) [32]. The AS has an important fiber amount of 85.43%, which makes it possible to say that this natural residue is adapted to obtain carbonaceous materials [33].

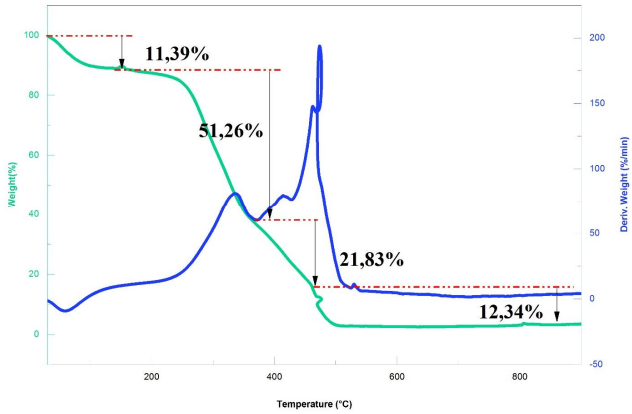

Fig. 6. TGA-DTG diagram of the Argan shells powder.

X-ray Diffraction Analysis

X-ray diffraction (XRD) study reveals the crystalline or amorphous properties of the material. Figure 7 gives the XRD diagram of AS-C92, in which we observe the appearance of two diffraction peaks, one at 24.33° and the other at 43.63°. These peaks inform us of the presence of graphitic reflections corresponding to the (0 0 2) and (1 0 0) planes. The peak that represents a higher intensity at 2θ = 24.33°, results from the parallel layer stacks. The peak at 2θ = 43.63° which represents a small intensity compared to the peak at 24.33° is related to the regular structure within the individual segments of the layer plane [34]. The diffractogram can also be used to describe the disordered carbon states characteristics [35].

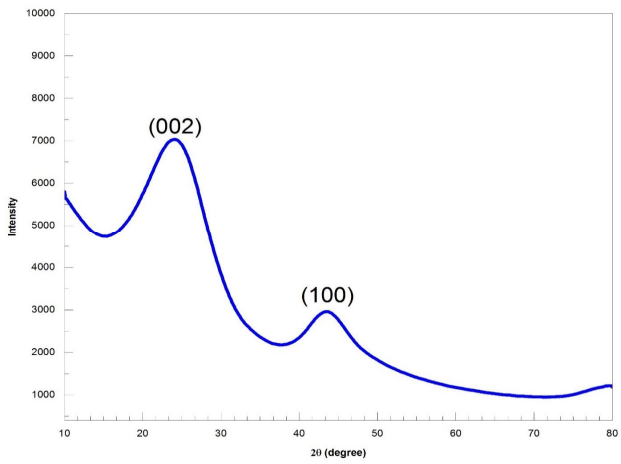

Fig. 7. XRD analysis of Biochar prepared from Argan shells powder.

Table 1 shows the values of interlayer spacing, d_{002}, and d_{100} where the distance of (002) and (100) planes is equal to

Table 1. The Crystal Structure Parameters of AS-C92

Sample	X-ray data				Crystallites size (nm)		Effective dimension (nm)
AS-C92	$2\theta_{002}$ (deg.)	$2\theta_{100}$ (deg.)	d_{002} (nm)	d_{100} (nm)	L_c	L_a	L'
	24.33	43.63	0.365	0.207	1.18	3.84	2.39

0.365 and 0.207 nm respectively. These values are different from the graphite value (0.335 nm) which shows that the crystallographic structure is still disordered and far from the complete graphitization.

The interlayer spacing d_{hkl} of AS-C92 was calculated using the Bragg equation:

$$d = \frac{\lambda}{2\sin\theta} \tag{4}$$

Where λ is the X-ray wavelength; θ is the Bragg angle. The values (L_a) and (L_c) corresponding to the width and height of crystallites along the a-axis and the c-axis, respectively, were determined using the Scherrer equation:

$$L = \frac{k\lambda}{\beta\cos\theta} \tag{5}$$

With L assigned to (L_c) or (L_a), β is the full width at half maximum of the peak and K is a form factor.

The effective dimension (L') was calculated using the following equation [36]:

$$L' = \left[\frac{\pi}{4} L_a^2 L_c\right]^{\frac{1}{3}} \tag{6}$$

Point of Zero Charge of AS-C92

The pH_{PZC} of material allows determines the pH at which the electrical charge on its surface is zero. This parameter is determined by a curve representing the difference of the initial and final pH (pH_0-pH_f) as a function of pH_0 values (Fig. 8). The intersection of this curve with the abscissa where the pH value is zero gives us the pH_{PZC}. The pH_{PZC} of AS-C92 from an aqueous solution is 8.4. At a pH value above 8.4, a strong electrostatic attraction could be generated by the difference in electrical charge between the surface of the material (negatively charged) and the molecules of the MB cationic dye (positively charged), which facilitates its movement to the surface and the adsorption becomes rapid.

Methylene Blue Adsorption

Effect of Biochar dose. To investigate the influence of AS-C92 dose on MB adsorption in aqueous solution,

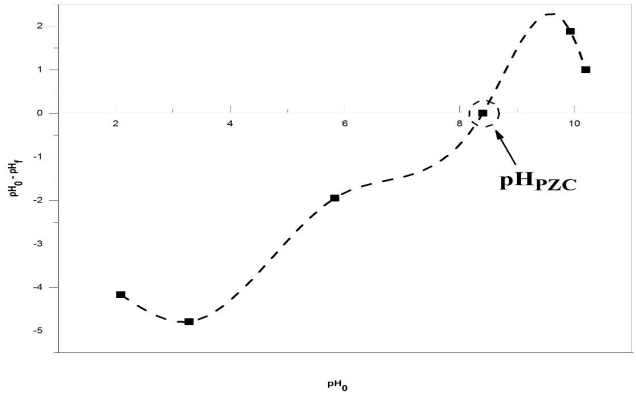

Fig. 8. Determination of the point of zero charges of AS-C92.

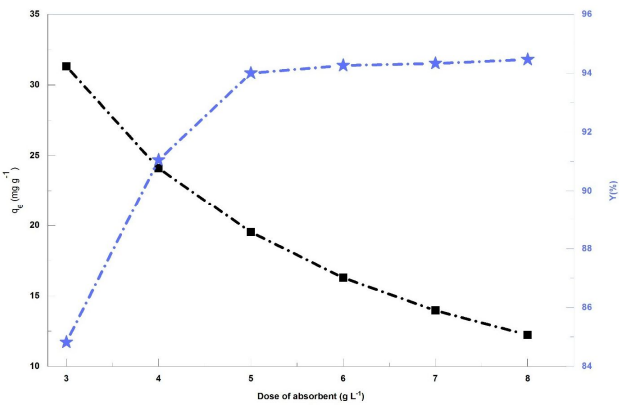

Fig. 9. The effect of AS-C92 dosage on MB adsorption (C_0 = 100 mg l^{-1}, T = 25 °C, contact time = 3 h, V = 100 ml, pH = 6.67).

manipulations were performed with a volume of 100 ml of MB solution (100 mg l^{-1}) to which different masses of AS-C92 were added: 0.3, 0.4, 0.5, 0.6, 0.7, and 0.8 g under a stirring speed of 400 rpm and contact time of 3 h. The results (Fig. 9) show that when the adsorbent dose increases, the yield of MB adsorption increases from 84, 82% for 0.3 g to 94.46% for 0.5 g; On the other hand, the adsorption capacity decreases from 31 to 12 mg g^{-1}, which explains the existence of a greater number of adsorption sites [37]. In addition, when the carbon dose is too high, the amount of adsorbed dye becomes constant. This can be explained by the large increase in carbon dose makes the sites unsaturated during the adsorption [38]. The dose of 5 g l^{-1} was

considered ideal for future experiments.

Effect of pH. The study of the effect of pH on the adsorption of MB on AS-C92 was performed at different pH values (from 1 to 10). The operating conditions were as follows: initial concentration of MB (100 mg l^{-1}), dosage of AS-C92 (0.5 g/100 ml), stirring speed (400 rpm), and contact time (3 h) at room temperature. The obtained results in Fig. 10 show that as the pH increases, the adsorption yield increases. The maximum adsorption of MB is 19.9 mg g^{-1} at pH 10. These results can be explained by surface charge of the adsorbent. At pH below pH_{PZC}, there are H^+ protons in the solution which compete with MB molecules; the AS-C92 surface adsorbs more H^+, which explains the reduced adsorption of MB molecules on the carbon surface. At pH above pH_{PZC}, there are negative charges on the adsorbent surface, which leads to the electrostatic attraction between the adsorbate (positive charges) and the adsorbent (negative charge), hence promoting the increase in the adsorption yield of MB [39].

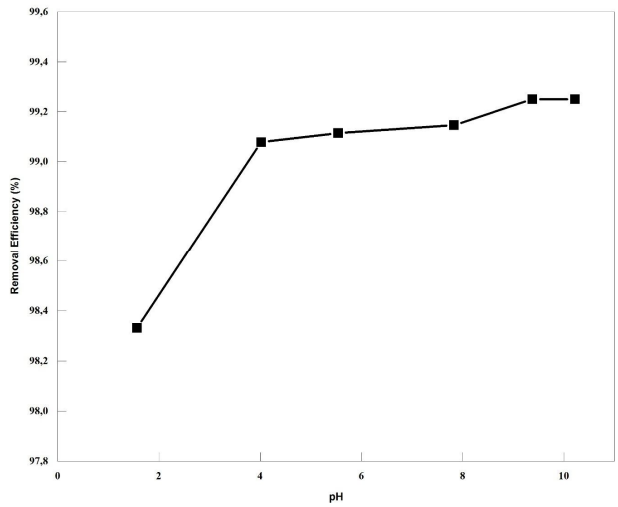

Fig. 10. The effect of the different pH on the removal of methylene blue (C_0 = 100 mg l^{-1}, T = 25 °C, contact time = 3 h, V = 100 ml, Biochar dose = 0.5 g l^{-1}).

Adsorption Isotherms

The qualitative data of adsorption isotherms can show the type of interaction between the adsorbate and the adsorbent surface, they also describe the distribution pattern of the adsorbent molecules between the liquid and solid phases at equilibrium state [40].

In this work, we treated three isotherms to describe the results obtained; the Temkin, the Freundlich, and the Langmuir isotherm.

The Langmuir model assumes adsorbate forms a monolayer on the adsorbent surface and absence of any interaction between the adsorbed molecules [41]. The experimental adsorption data can be fitted with this model to estimate the adsorption mechanism according to the following equation [42] :

$$\frac{C_e}{q_e} = \frac{1}{q_m K_L} + \frac{C_e}{q_m} \tag{7}$$

Where C_e is the dye concentration at equilibrium (mg l^{-1}), q_e is the amount of dye adsorbed at equilibrium (mg g^{-1}), q_m is monolayer adsorption capacity (mg g^{-1}), and K_L is the isotherm constant (l mg^{-1}).

The dimensionless separation factor R_L can express the essential features of the Langmuir isotherm [43], It can be calculated using the following equation :

$$R_L = \frac{1}{1 + K_L C_0} \tag{8}$$

Where K_L is the Langmuir constant and C_0 is the initial dye concentration (mg l^{-1}).

The Freundlich model is applied in the case of multilayer adsorption. In this model of the interactions are likely to be present between the adsorbed molecules. The Freundlich isotherm is given by the following equation [44] :

$$\ln q_e = \frac{1}{n} \ln C_e + \ln K_F \tag{9}$$

Where K_F (l mg^{-1}) and n are the Freundlich adsorption constants.

The effects of interactions adsorbate-adsorbate on the adsorption isotherm are shown by the Temkin model. This model suggests a linear decrease in the heat of the adsorbed molecules.

The Temkin isotherm can be presented in the form [45]:

$$q_e = \frac{RT}{b} \ln(AC_e) \tag{10}$$

Where A (l mg^{-1}) and b (J mol^{-1}) are the Temkin isotherm constants, R (8.314 J mol^{-1} K^{-1}) is the universal gas constant and T (K) is the absolute temperature.
The Eq. (10) can be linearized as:

$$q_e = B \ln A + B \ln C_e \tag{11}$$

Where $B = \frac{RT}{b}$

The experimental data of the adsorption isotherm of the three models are presented in Fig. 11. The parameters of the isotherm and the correlation coefficient R^2, which represent the fitting results, are indicated in Table 2. The obtained value of R_L for MB adsorption ($R_L < 1$) we deduce that Biochar has a favorable adsorption interaction toward the dye [46]. According to the linear regression method, the Langmuir isotherm is better fitted (R^2 = 0.9983) than the Freundlich and Temkin isotherms for the MB adsorption on AS-C92. This result shows that the MB molecules formed a monolayer on the biochar surface and the activation energy is the same for the adsorption of each molecule.

Adsorption Kinetics

In order to study the relationship between the adsorption capacity of the adsorbent and the contact time, the pseudo-first-order model, the pseudo-second-order model, and the intraparticle diffusion model, are the three models used to describe the reaction order of MB adsorption on AS-C92.

The pseudo-first-order model is given by the following Lagergren equation [47] :

$$\frac{dq_t}{dt} = K_1(q_e - q_t) \tag{12}$$

q_e and q_t are the adsorbed quantities of MB (mg g^{-1}) at equilibrium and time t, respectively. K_1 represents the pseudo-first-order rate constant (min^{-1}).
With integration at initial conditions ($t = 0$, $q_t = 0$ and $t = t_e$, $q_t = q_e$), equation 12 becomes:

$$\ln(q_e - q_t) = \ln(q_e) - k_1 t \tag{13}$$

The kinetic data were then presented with the pseudo-second-order kinetic model [48]. The differential equation representing this model is as follows:

$$\frac{dq_t}{dt} = k_2(q_e - q_t)^2 \tag{14}$$

K_2 represents the pseudo-second-order rate constant (g mg^{-1} min^{-1}).

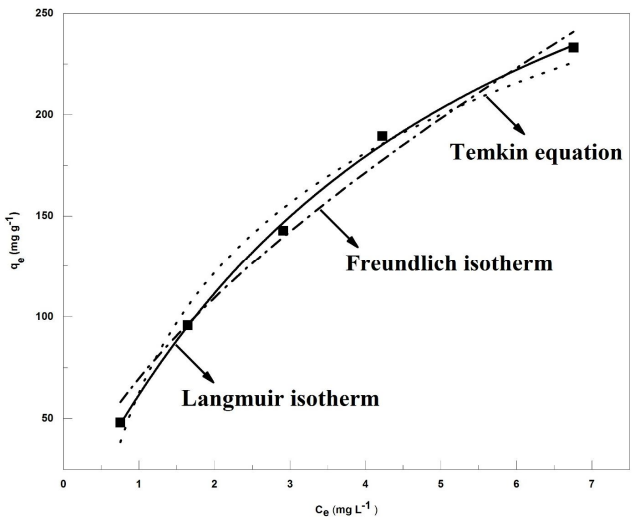

Fig. 11. Plots of isotherm models for the adsorption of MB adsorption on AS-C92 (T = 25 °C , V = 100 ml, contact time = 2 h, Biochar dose = 0.5 g l^{-1}, pH = 10).

Table 2. Equilibrium Model Parameters for Adsorption of MB onto Optimal Biochar

Isotherm	Parameters	Value
Langmuir	q_m(mg g^{-1})	31
	K_L(l mg^{-1})	0.19
	R^2	0.9983
	R_L	0.058
Freundlich	K_F (mg g^{-1})	5.56
	n	1.54
	R^2	0.9855
Temkin	A(l g^{-1})	2.08
	B(J mol^{-1})	6.83
	R^2	0.9828

With integration at initial conditions ($t = 0$, $q_t = 0$ and $t = t_e$, $q_t = q_e$), Eq. (14) becomes:

$$\frac{t}{q_t} = \frac{1}{(k_2 q_e^2)} + \frac{1}{q_e} t \tag{15}$$

The intraparticle diffusion model is given by the following equation [49] :

$$q_t = k_{dif}\, t^{\frac{1}{2}} \tag{16}$$

Where K_{dif} is the intraparticle diffusion rate constant (mg (g min$^{1/2}$)$^{-1}$).

Figure 12 shows the presentation of the pseudo-first-order and the pseudo-second-order kinetic models and the intraparticle diffusion plot, q_t *vs*. $t^{1/2}$ is shown in Fig. 13.

The results obtained in Figs. 12 and 13 show that the adsorption kinetics conforms to a pseudo-second-order equation. From Table 3, the calculated values of q_e ($q_{e,c}$) are in agreement with the experimental values of q_e ($q_{e,e}$) and the value of the correlation coefficient R^2 is equal to 1. From these results, we can deduce that the studied adsorption system well meets the pseudo-second-order kinetic model.

However, the intra-particle diffusion plot (Fig. 13) displays a multi-linear fit. This behavior shows that the adsorption process involved two steps [49]. The first one corresponds to dye diffusion through the solution to the external surface of the adsorbents. The second stage may be attributed to the gradual adsorption of MB onto AS-C92 [50].

CONCLUSIONS

The results of this work showed that the Biochar prepared from Argan shells by the thermal activation method with temperature from 500 °C to 900 °C has a well-developed porosity. The study of the effects of carbonization parameters on Burn-off and iodine number, as well as the study of the adsorption properties of MB on the prepared AS-C92, have shown a significant increase in adsorption yield. The pH_{pzc} of the AS-C92 prepared at the optimal conditions of 900 °C for 2 h was 8.3. SEM images

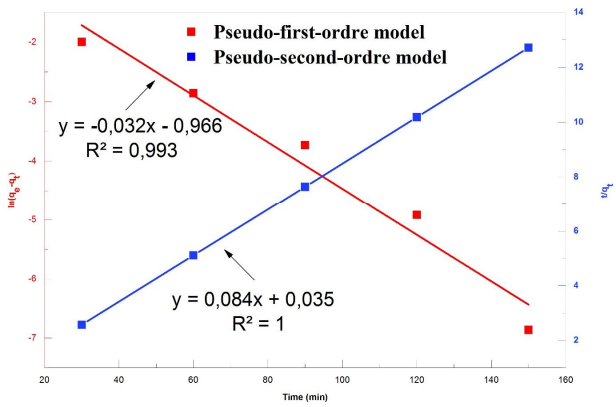

Fig. 12. The kinetic models for adsorption of MB on AS-C92, Pseudo-first-order model, and Pseudo-second-order model.

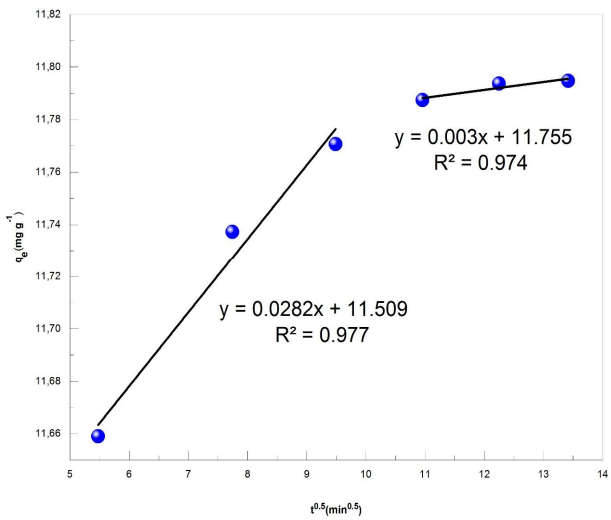

Fig. 13. Intraparticle diffusion model.

Table 3. Kinetic Model Parameters for the Adsorption of MB on AS-C92

Pseudo-second order model				
Initial concentration (mg l^{-1})	$q_{e,e}$ (mg g^{-1})	K_2 (l mg^{-1} min^{-1})	$q_{e,c}$ (mg g^{-1})	R^2
100	19.79	0.4	19.84	1

showed that the BC had a surface that contained full of cavities in relation to the AS. Dye adsorption is maximal in the pH range between 9.0 and 10.0. The isothermal model best suited for the MB adsorption on the material surface is the Langmuir model. The values of q_m and K_L found by the Langmuir model are 31 mg g^{-1} and 0.19 l mg^{-1}, respectively. According to the experimental results, the Biochar produced from the Argan shells is expected to be an economical adsorbent for dyes remediation from water and wastewater.

REFERENTES

[1] Vaddi, D.; Subbarao, M. V.; Muralikrishna, M. P. S., Removal of manganese(II) from aqueous solution by chemically activated Thuja Occidentalis leaves carbon (CATLC) as an adsorbent: Adsorption equilibrium and kinetic studies. *Phys. Chem. Res.* **2019**, *7*, 11-26, DOI: 10.22036/pcr.2018.149256.1539.

[2] Pathania, D.; Sharma, S.; Singh, P., Removal of methylene blue by adsorption onto activated carbon developed from Ficus carica bast. *Arab. J. Chem.* **2017**, *10*, S1445-S1451, DOI: 10.1016/j.arabjc.2013.04.021.

[3] Chegeni, M.; Etemadpour, S.; Fekri, M. H., The perlite-calcium alginate-activated carbon composite as an efficient adsorbent for the removal of dyes from aqueous solutions. *Phys. Chem. Res.* **2021**, *9*, 1-16, DOI: 10.22036/pcr.2020.232973.1779.

[4] Eltaweil, A. S.; Elgarhy, G. S.; El-Subruiti, G. M.; Omer, A. M., Carboxymethyl cellulose/carboxylated graphene oxide composite microbeads for efficient adsorption of cationic methylene blue dye. *Int. J. Biol. Macromol.* **2020**, *154*, 307-318, DOI: 10.1016/j.ijbiomac.2020.03.122.

[5] Mohammadiyan, E.; Ghafuri, H.; Kakanejadifard, A., Optik Synthesis and characterization of a magnetic Fe_3O_4@CeO_2 nanocomposite decorated with Ag nanoparticle and investigation of synergistic effects of Ag on photocatalytic activity. *Opt.- Int. J. Light Electron Opt.* **2018**, *166*, 39-48, DOI: 10.1016/j.ijleo.2018.03.044.

[6] Tharaneedhar, V.; Kumar, P. S.; Saravanan, A.; Ravikumar, C.; Jaikumar, V., Prediction and interpretation of adsorption parameters for the sequestration of methylene blue dye from aqueous solution using microwave assisted corncob activated carbon. *SUSMAT.* **2016**, *11*, 1-11, DOI: 10.1016/j.susmat.2016.11.001.

[7] Ahmad, A. L.; Loh, M. M.; Aziz, J. A., Preparation and characterization of activated carbon from oil palm wood and its evaluation on Methylene blue adsorption. *Dye. Pigment.* **2007**, *75*, 263-272, DOI: 10.1016/j.dyepig.2006.05.034.

[8] Deng, H.; Yang, L.; Tao, G.; Dai, J., Preparation and characterization of activated carbon from cotton stalk by microwave assisted chemical activation-application in methylene blue adsorption from aqueous solution. *J. Hazard. Mater.* **2009**, *166*, 1514-1521, DOI: 10.1016/j.jhazmat.2008.12.080.

[9] Namasivayam, C.; Sangeetha, D., Recycling of agricultural solid waste, coir pith : Removal of anions , heavy metals, organics and dyes from water by adsorption onto $ZnCl_2$ activated coir pith carbon. *J. Hazard. Mater.* **2006**, *135*, 449-452, DOI: 10.1016/j.jhazmat.2005.11.066.

[10] Enniya, I.; Rghioui, L.; Jourani, A., Adsorption of hexavalent chromium in aqueous solution on activated carbon prepared from apple peels. *Sustain. Chem. Pharm.* **2018**, *7*, 9-16, DOI: 10.1016/j.scp.2017.11.003.

[11] Zhu, Y.; Kolar, P.; Shah, S. B.; Cheng, J. J.; Lim, P. K., Avocado seed-derived activated carbon for mitigation of aqueous ammonium. *Ind. Crops Prod.* **2016**, *92*, 34-41, DOI: 10.1016/j.indcrop.2016.07.016.

[12] Garg, D.; Kumar, S.; Sharma, K.; Majumder, C. B., Groundwater for sustainable development application of waste peanut shells to form activated carbon and its utilization for the removal of acid y/ellow 36 from wastewater. *Groundw. Sustain. Dev.* **2019**, *8*, 512-519, DOI: 10.1016/j.gsd.2019.01.010.

[13] Zyoud, A.; Nassar, H. N. I.; El-hamouz, A.; Hilal, H. S., Solid olive waste in environmental cleanup : Enhanced nitrite ion removal by $ZnCl_2$-activated carbon. *J. Environ. Manage.* **2015**, *152*, 27-35, DOI: 10.1016/j.jenvman.2015.01.001.

[14] Jain, A.; Tripathi, S. K., Nano-porous activated carbon from sugarcane waste for supercapacitor application. *J. Energy Storage.* **2015**, *4*, 121-127, DOI: 10.1016/

j.est.2015.09.010.

[15] Khallouki, F. *et al.*, Identification of polyphenolic compounds in the flesh of Argan (Morocco) fruits. *Food Chem.* **2015**, *179*, 191-198, DOI: 10.1016/j.foodchem.2015.01.103.

[16] Karim, M. M.; Das, A. K.; Lee, S. H., Treatment of colored effluent of the textile industry in Bangladesh using zinc chloride treated indigenous activated carbons. *Anal. Chim. Acta.* **2006**, *576*, 37-42, DOI: 10.1016/j.aca.2006.01.079.

[17] aka, C., BET, TG-DTG, FT-IR, SEM, iodine number analysis and preparation of activated carbon from acorn shell by chemical activation with $ZnCl_2$. *J. Anal. Appl. Pyrolysis.* **2012**, *95*, 21-24, DOI: 10.1016/j.jaap.2011.12.020.

[18] Kumar, A.; Prasad, B.; Mishra, I. M., Adsorptive removal of acrylonitrile by commercial grade activated carbon: Kinetics, equilibrium and thermodynamics. *J. Hazard. Mater.* **2008**, *152*, 589-600, DOI: 10.1016/j.jhazmat.2007.07.048.

[19] Farahani, M.; Abdullah, S. R. S.; Hosseini, S.; Shojaeipour, S.; Kashisaz, M., Adsorption-based cationic dyes using the carbon active sugarcane bagasse. *Procedia Environ. Sci.* **2011**, *10*, 203-208, DOI: 10.1016/j.proenv.2011.09.035.

[20] Başar, C. A., Applicability of the various adsorption models of three dyes adsorption onto activated carbon prepared waste apricot. *J. Hazard. Mater.* **2006**, *135*, 232-241, DOI: 10.1016/j.jhazmat.2005.11.055.

[21] Hu, Z.; Srinivasan, M. P., Mesoporous high-surface-area activated carbon. *Microporous Mesoporous Mater.* **2001**, *43*, 267-275, DOI: 10.1016/S1387-1811(00)00355-3.

[22] Wartelle, L. H.; Marshall, W. E.; Toles, C. A.; Johns, M. M., Comparison of nutshell granular activated carbons to commercial adsorbents for the purge-and-trap gas chromatographic analysis of volatile organic compounds. *J. Chromatogr. A.* **2000**, *879*, 169-175, DOI: 10.1016/S0021-9673(00)00290-9.

[23] Ogungbenro, A. E.; Quang, D. V.; Al-Ali, K.; Abu-Zahra, M. R. M., Activated carbon from date seeds for CO_2 capture applications. *Energy Procedia.* **2017**, *114*, 2313-2321, DOI: 10.1016/j.egypro.2017.03.1370.

[24] Bouhamed, F.; Elouear, Z.; Bouzid, J., Adsorptive removal of copper(II) from aqueous solutions on activated carbon prepared from Tunisian date stones: Equilibrium, kinetics and thermodynamics. *J. Taiwan Inst. Chem. Eng.* **2012**, *43*, 741-749, DOI: 10.1016/j.jtice.2012.02.011.

[25] Aguilar, C.; García, R.; Soto-Garrido, G.; Arriagada, R., Catalytic wet air oxidation of aqueous ammonia with activated carbon. *Appl. Catal. B Environ.* **2003**, *46*, 229-237, DOI: 10.1016/S0926-3373(03)00229-7.

[26] N. González, M. J. F.-B., Fourier transform infrared spectroscopy in the study of the interaction between PVC and plasticizers: PVC/plasticizer compatibility. *J. Appl. Polym. Sci.* **2007**, *116*, 2658-2667, DOI: 10.1002/app.

[27] Yu, Z.; Zhou, J.; Zhang, J.; Huang, K.; Cao, F.; Wei, P., Evaluating effects of biobased 2,5-furandicarboxylate esters as plasticizers on the thermal and mechanical properties of poly (vinyl chloride). *J. Appl. Polym. Sci.* **2014**, *131*, 1-10, DOI: 10.1002/app.40938.

[28] Boonamnuayvitaya, V.; Sae-Ung, S.; Tanthapanichakoon, W., Preparation of activated carbons from coffee residue for the adsorption of formaldehyde. *Sep. Purif. Technol.* **2005**, *42*, 159-168, DOI: 10.1016/j.seppur.2004.07.007.

[29] Yang, H.; Yan, R.; Chen, H.; Lee, D. H.; Zheng, C., Characteristics of hemicellulose, cellulose and lignin pyrolysis. *Fuel.* **2007**, *86*, 1781-1788, DOI: 10.1016/j.fuel.2006.12.013.

[30] Deng, H.; Li, G.; Yang, H.; Tang, J.; Tang, J., Preparation of activated carbons from cotton stalk by microwave assisted KOH and K_2CO_3 activation. *Chem. Eng. J.* ***2010***, *163*, 373-381, DOI: 10.1016/j.cej.2010.08.019.

[31] Bedin, K. C.; Martins, A. C.; Gazetta A. L.; Pezoti, O.; Pezoti, O.; Almeida, V. C., KOH-activated carbon prepared from sucrose spherical carbon: adsorption equilibrium, kinetic and thermodynamic studies for methylene blue removal. *Chem. Eng. J.* **2016**, *286*, 476-484, DOI: 10.1016/j.cej.2015.10.099.

[32] El Abbari, H. *et al.*, Thermal and thermomechanical behavior of moroccan Boufeggous variety date seeds. *J. Therm. Anal. Calorim.* **2019**, *137*, 1485-1492,

DOI: 10.1007/s10973-019-08060-8.

[33] Sim, C. K.; Majid, S. R.; Mahmood, N. Z., Durable porous carbon/$ZnMn_2O_4$ composite electrode material for supercapacitor. *J. Alloys Compd.* **2019**, *803*, 424-433, DOI: 10.1016/j.jallcom.2019.06.220.

[34] Hadoun, H.; Sadaoui, Z.; Souami, N.; Sahel, D.; Toumert, I., Characterization of mesoporous carbon prepared from date stems by H_3PO_4 chemical activation. *Appl. Surf. Sci.* **2013**, *280*, 1-7, DOI: 10.1016/j.apsusc.2013.04.054.

[35] Schmidt, W., Calculation of XRD patterns of simulated FDU-15, CMK-5, and CMK-3 carbon structures. *Microporous Mesoporous Mater.* **2009**, *117*, 372-379, DOI: 10.1016/j.micromeso.2008.07.020.

[36] Ma, X.; Zhang, F.; Zhu, J.; Yu, L.; Liu, X., Preparation of highly developed mesoporous activated carbon fiber from liquefied wood using wood charcoal as additive and its adsorption of methylene blue from solution. *Bioresour. Technol.* **2014**, *164*, 1-6, DOI: 10.1016/j.biortech.2014.04.050.

[37] Khajeh, M.; Nemch, T. K., Determination of chromium and nickel in water samples by zinc oxide nanoparticle-chitosan: Equilibrium, kinetic and thermodynamic studies. *J. Anal. Test.* **2018**, *2*, 299-305, DOI: 10.1007/s41664-018-0067-3.

[38] Desta, M. B., Batch sorption experiments: Langmuir and freundlich isotherm studies for the adsorption of textile metal ions onto teff straw (Eragrostis tef) agricultural waste. *J. Thermodyn.* **2013**, *2013*, 1-6, DOI: 10.1155/2013/375830.

[39] Shukla, S. S.; Li, J. Y.; Dorris, K. L.; Shukla, A., Removal of nickel from aqueous solutions by sawdust. *J. Hazard. Mater.* **2005**, *121*, 243-246, DOI: 10.1016/j.jhazmat.2004.11.025.

[40] Li, K.; Zheng, Z.; Huang, X.; Zhao, G.; Feng, J.; Zhang, J., Equilibrium, kinetic and thermodynamic studies on the adsorption of 2-nitroaniline onto activated carbon prepared from cotton stalk fibre. *J. Hazard. Mater.* **2009**, *166*, 213-220, DOI: 10.1016/j.jhazmat.2008.11.007.

[41] Xia, Y.; Yao, Q.; Zhang, W.; Zhang, Y.; Zhao, M., Comparative adsorption of methylene blue by magnetic baker's yeast and EDTAD-modified magnetic baker's yeast: Equilibrium and kinetic study. *Arab. J. Chem.* **2015**, *12*, 2448-2456, DOI: 10.1016/j.arabjc.2015.03.010.

[42] Niaei, H. A.; Rostamizadeh, M.; Maasumi, F.; Darabi, M. J., Kinetic, isotherm, and thermodynamic studies of methylene blue adsorption over metal-doped zeolite nano-adsorbent. *Phys. Chem. Res.* **2021**, *9*, 17-30, DOI: 10.22036/pcr.2020.233844.1781.

[43] Ait Himi, M.; El Ghachtouli, S.; Amarray, A.; Zaroual, Z.; Bonnaillie, P.; Azzi, M., Removal of azo dye Calcon using polyaniline films electrodeposited on SnO_2 substrate. *Phys. Chem. Res.* **2020**, *8*, 111-124, DOI: 10.22036/pcr.2019.203023.1680.

[44] Karnib, M.; Kabbani, A.; Holail, H.; Olama, Z., Heavy metals removal using activated carbon, silica and silica activated carbon composite. *Energy Procedia.* **2014**, *50*, 113-120, DOI: 10.1016/ j.egypro.2014.06.014.

[45] Pandiarajan, A.; Kamaraj, R.; Vasudevan, S.; Vasudevan, S., OPAC (orange peel activated carbon) derived from waste orange peel for the adsorption of chlorophenoxyacetic acid herbicides from water: Adsorption isotherm, kinetic modelling and thermodynamic studies. *Bioresour. Technol.* **2018**, *261*, 329-341, DOI: 10.1016/j.biortech.2018.04.005.

[46] Zou, C.; Jiang, W.; Liang, J.; Sun, X.; Guan, Y., Removal of Pb(II) from aqueous solutions by adsorption on magnetic bentonite. *Environ. Sci. Pollut. Res.* **2019**, *26*, 1315-1322, DOI: 10.1007/s11356-018-3652-0.

[47] Demiral, H.; Güngör, C., Adsorption of copper(II) from aqueous solutions on activated carbon prepared from grape bagasse. *J. Clean. Prod.* **2016**, *124*, 103-113, DOI: 10.1016/j.jclepro.2016.02.084.

[48] Li, K.; Wang, X., Adsorptive removal of Pb(II) by activated carbon prepared from Spartina alterniflora: Equilibrium, kinetics and thermodynamics. *Bioresour. Technol.* **2009**, *100*, 2810-2815, DOI: 10.1016/j.biortech.2008.12.032.

[49] Salari, H.; Erami, M.; Dokoohaki, M. H.; Zolghadr, A. R., New insights into adsorption equilibrium of organic pollutant on MnO_2 nanorods: Experimental and computational studies. *J. Mol. Liq.* **2021**, Vol. ?, 117016, DOI: 10.1016/j.molliq.2021.117016.

[50] Chaabane, L.; Beyou, E.; El Ghali, A.; Baouab, M. H. V., Comparative studies on the adsorption of metal ions from aqueous solutions using various functionalized graphene oxide sheets as supported adsorbents. *J. Hazard. Mater.* **2020**, *389*, 121839, DOI: 10.1016/j.jhazmat.2019.121839.